JACS
JOURNAL OF THE AMERICAN CHEMICAL SOCIETY

ARTICLE

pubs.acs.org/JACS

Multicompartment Polymer Nanostructures with Ratiometric Dual-Emission pH-Sensitivity

Guorong Sun,[†] Honggang Cui,[‡] Lily Yun Lin,[†] Nam S. Lee,[†] Chao Yang,[†] William L. Neumann,[§] John N. Freskos,[∥] Jeng J. Shieh,[∥] Richard B. Dorshow,[∥] and Karen L. Wooley*[,†]

[†]Department of Chemistry and Department of Chemical Engineering, Texas A&M University, College Station, Texas 77842, United States

[‡]Department of Chemical and Biomolecular Engineering, Johns Hopkins University, Baltimore, Maryland 21218, United States

[§]Department of Pharmaceutical Sciences, Southern Illinois University Edwardsville School of Pharmacy, Edwardsville, Illinois 62026, United States

[∥]Covidien Pharmaceutical R&D, Hazelwood, Missouri 63042, United States

Supporting Information

ABSTRACT: Pyrazine-labeled multicompartment nanostructures are shown to exhibit enhanced pH-responsive blue-shifted fluorescence emission intensities compared to their simpler core−shell spherical analogs. An amphiphilic linear triblock terpolymer of ethylene oxide, *N*-acryloxysuccinimide, and styrene, PEO_{45}-*b*-$PNAS_{105}$-*b*-PS_{45}, which lacks significant incompatibility for the hydrophobic block segments and undergoes gradual hydrolysis of the NAS units, underwent supramolecular assembly in mixtures of organic solvent and water to afford multicompartment micelles (MCMs) with a narrow size distribution. The assembly process was followed over time and found to evolve from individual polymer nanodroplets containing internally phase segregated domains, of increasing definition, and ultimately to dissociate into discrete micelles. Upon covalent cross-linking of the MCMs with pH-insensitive pyrazine-based diamino cross-linkers, pH-responsive, photonic multicompartment nanostructures (MCNs) were produced. These MCNs exhibited significant enhancement of overall structural stability, in comparison with the MCMs, and internal structural tunability through the cross-linking chemistry. Meanwhile, the complex compartmentalized morphology exerted unique pH-responsive fluorescence dual-emission properties, indicating promise in ratiometric pH-sensing applications.

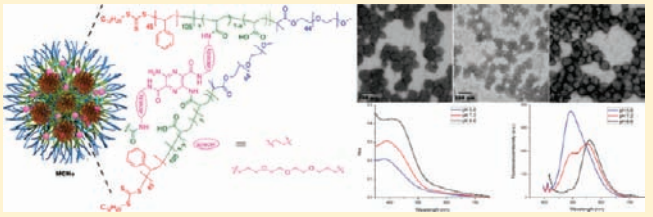

INTRODUCTION

The development of polymeric nanostructures from block copolymer supramolecular assemblies has gained significant attention,[1−11] from which it has been recognized that their chemical composition, size, and morphology each require precise tuning. Inspired by the successes from small molecule amphiphiles such as lipids, considerable efforts have been devoted to understand and manipulate the aqueous self-assembly process of amphiphilic block copolymers to obtain nanoscale assemblies with complex morphologies, which has been demonstrated as a promising parameter for addressing their potential biomedical applications.[12−15] For example, nonspherical nanostructures exhibited prolonged blood circulation time,[16] more proficient cell targeting,[17] and more efficient phagocytosis,[18] compared with the corresponding spherical counterparts. Benefiting from the advances of living/controlled polymerization methodologies to afford varied block copolymer structures,[19−24] together with extensive investigation of their aqueous assembly,[22,25−34] polymeric nanostructures with diverse morphologies have been established. In addition to conventional morphologies, such as spheres, cylinders, and vesicles, bowls,[35] discs,[36] helices,[37] and toroids[38] have been reported. Moreover, Janus,[39] multicompartment,[40,41] onion,[42] and large compound micelles,[43] from higher-order inter- and/or intramicellar phase segregation, have been created.

Multicompartment micelles (MCMs) represent intramicellar phase-segregated block copolymer supramolecular assemblies, in which the core domains are heterogeneous and compartmentalized.[25,44] Utilizing ABC starlike block terpolymers, by Lodge, Hillmyer and co-workers,[40] and ABC linear triblock copolymers, by Laschewsky et al.[41] (in both cases, A represents the hydrophilic block segment, and B and C represent incompatible hydrophobic block segments), MCMs were realized through the compartmentalization of B and C blocks during the aqueous assembly process. Additional MCMs have been prepared by tuning of polymeric and supramolecular parameters to manipulate the sizes, morphologies,[45−53] and internal environments of the compartmentalized cores[54−57] and to generate stimuli-induced responses.[58−61] Meanwhile, the performance of MCMs as

Received: May 26, 2010
Published: May 16, 2011

Scheme 1. Construction of Photophysically Functionalized MCNs by Supramolecular Assembly of Triblock Terpolymers in Solution Followed by Cross-linking with Chromophores

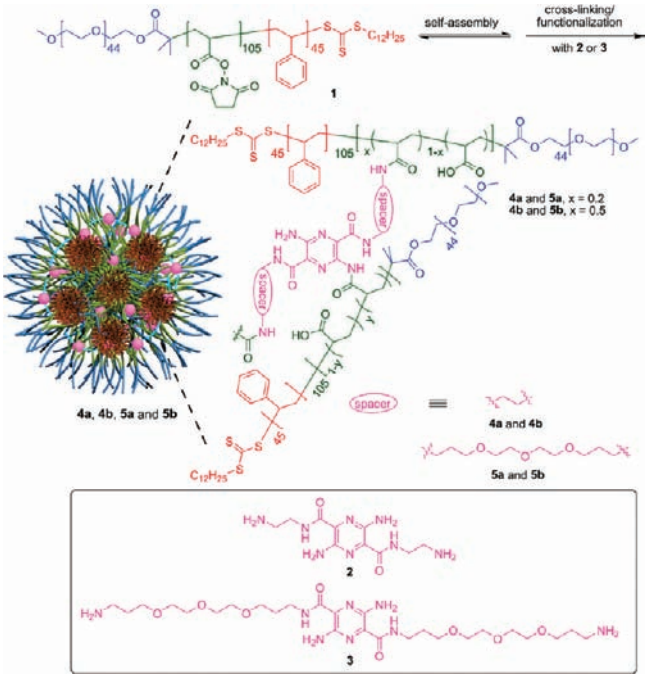

delivery vehicles for various cargos has been investigated to address their unique potential for biomedical applications.[62]

Whereas a variety of star terpolymers[40,45−48,54,56,58,60] and linear block copolymers[41,50−53,55,57,61,63] have been explored as precursors to prepare MCMs, the introduction of functionalities into MCMs for facile and practical chemical manipulations[64,65] remains as a fundamental aspect requiring further investigation.[52] Here, we report our approach for the construction of MCMs from the aqueous assembly of a linear poly(ethylene oxide)-*block*-poly(*N*-acryloxysuccinimide)-*block*-polystyrene (PEO-*b*-PNAS-*b*-PS), **1**, amphiphilic ABC triblock terpolymer, to afford nanoscopic assemblies with compartmentalized PS core domains. Borrowing from the terminology that has been developed for multivalent systems, which can be of either homomultivalency or heteromultivalency,[66] we adopt the term "multicompartment", for these newly developed homomulticompartment materials. The overall process involves an evolution from individual nanodroplets of polymer dispersed in water, to increasingly defined phase-segregated domains within those nanodroplets, and ultimately to discrete micelles, as the NAS functionalities undergo hydrolysis over time. While still present, the residual NAS functionalities within MCMs can be utilized for covalent incorporation of other molecules to render the MCMs functionalized, through well-established amidation chemistry.

In this study, photophysically active pyrazine-based diamino cross-linkers, **2** or **3** (Scheme 1), were used to establish the stabilized photoactive multicompartment nanostructures (MCNs), **4a**, **4b**, **5a**, and **5b**, respectively. The cross-linking not only enhances the stability of MCMs to afford MCNs with hydrophilic shells but also allows for tuning of the MCN internal spacing, through varying the chemical structures and the incorporation stoichiometry of the cross-linkers. These MCNs exhibit unique fluorescence emission characteristics, upon exposure to external environments at different pH values.

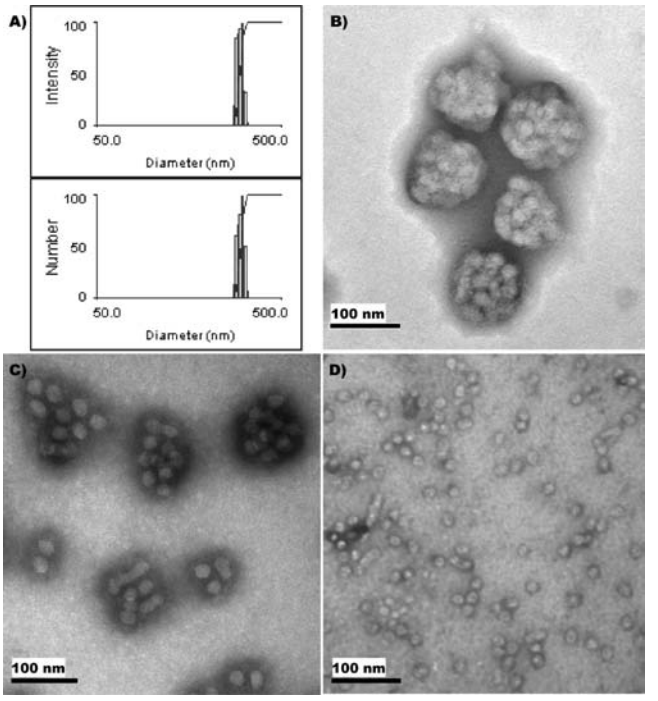

Figure 1. Characterization of MCMs in DMF/H_2O (v/v = 1:1, polymer concentrations were ~0.5 mg/mL). (A) Intensity-average weighted (top) and number-average weighted (bottom) hydrodynamic diameter distribution of "as prepared" MCMs by DLS (the scale of *x*-axis was presented by logarithmic). (B) TEM image (collected after drop deposition onto carbon-coated copper grids) of "as prepared" MCMs after 24 h of storage at room temperature (stained negatively with PTA). (C) TEM image of "as prepared" MCMs without any covalent stabilization after 3 months of storage at room temperature (stained negatively with PTA). (D) TEM image of "as prepared" MCMs without any covalent stabilization after 9 months of storage at room temperature (stained negatively with PTA).

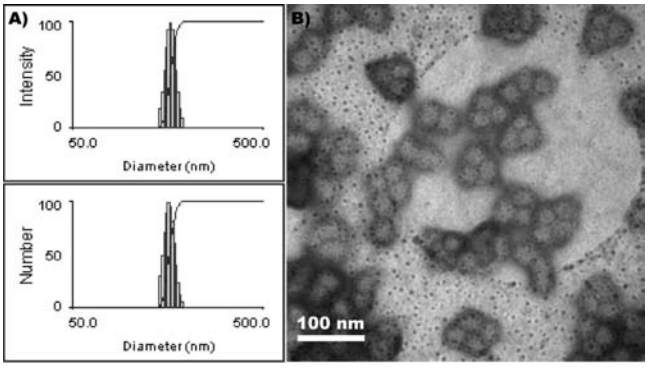

Figure 2. Small MCMs assembled from PEO_{45}-*b*-P(NAS_{95}-*co*-AA_{10})-*b*-PS_{45} precursors in DMF/H_2O (v/v = 1:1, polymer concentrations were ~0.5 mg/mL). (A) Intensity-average weighted (top) and number-average weighted (bottom) hydrodynamic diameter distribution of "as prepared" MCMs by DLS (the scale of *x*-axis was presented by logarithmic). (B) TEM image (collected after drop deposition onto carbon-coated copper grids) of "as prepared" MCMs after 24 h of storage at room temperature (stained negatively with PTA).

dx.doi.org/10.1021/ja200182t |*J. Am. Chem. Soc.* 2011, 133, 8534–8543

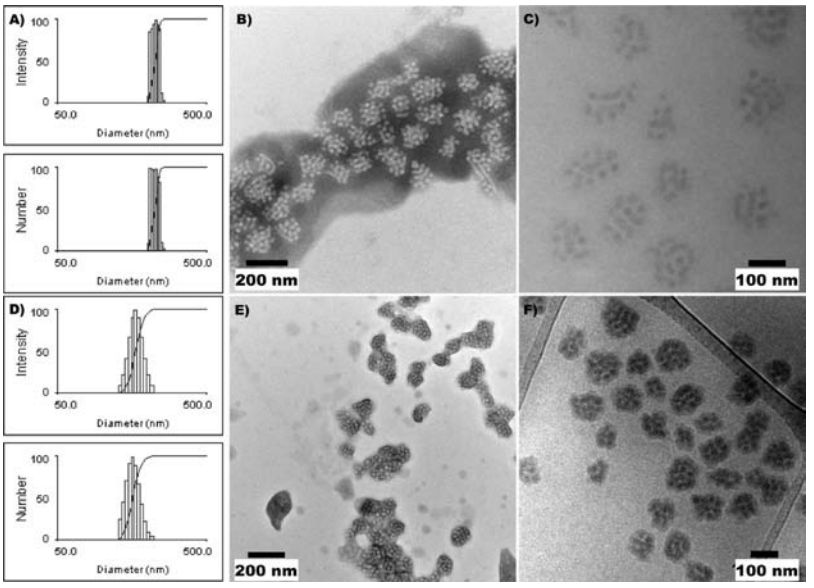

Figure 3. Characterization of MCNs prepared from PEO_{45}-*b*-$PNAS_{105}$-*b*-PS_{45} precursors and cross-linked with **2** in pH 7.2, 5 mM PBS buffer (with 5 mM of NaCl, polymer concentrations were 0.2−0.3 mg/mL). (A−C) and (D−F) Hydrodynamic diameter histograms as measured by DLS (the scale of *x*-axis was presented by logarithmic), TEM micrograph (stained negatively with PTA), and cryogenic TEM micrograph of **4a** and **4b**, respectively.

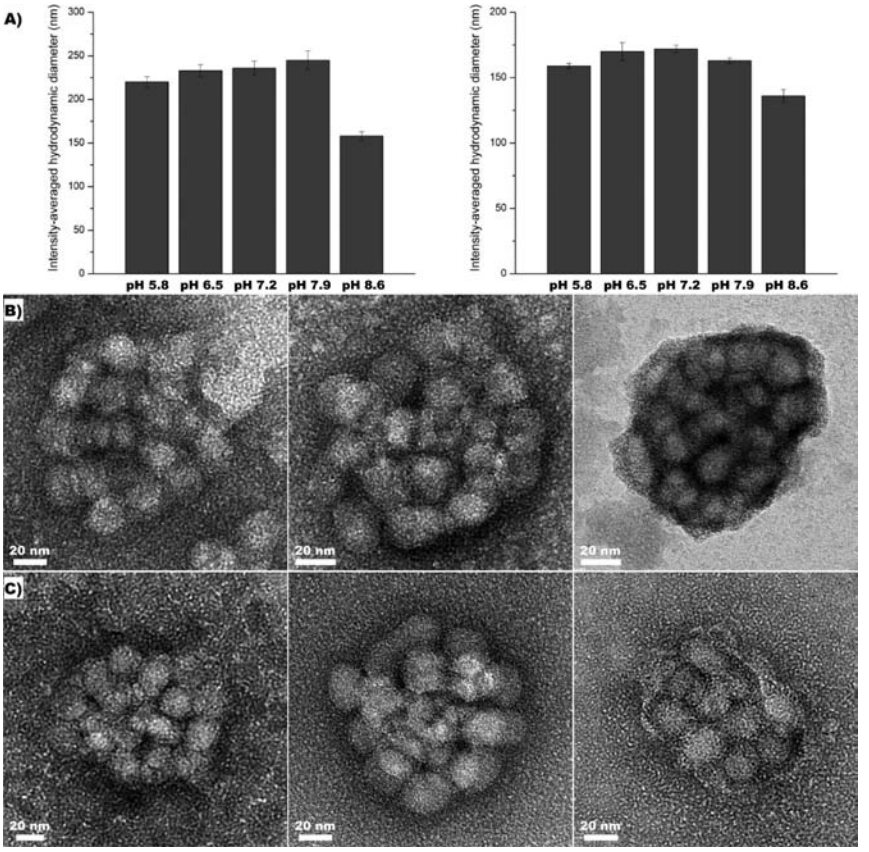

Figure 4. Characterization of MCNs (**4a** and **4b**, polymer concentrations were 0.2−0.3 mg/mL) cross-linked/functionalized by **2**. (A) DLS histograms of intensity-averaged hydrodynamic diameters for **4a** (left) and **4b** (right) in buffer solutions (5 mM with 5 mM of NaCl) at different pH values. (B) High-resolution TEM micrographs (stained negatively with PTA) of **4a** collected after drop deposition onto carbon-coated copper grids from pH 5.8 (left), pH 7.2 (middle), and pH 8.6 (right) buffer solutions (5 mM with 5 mM of NaCl), respectively. (C) High-resolution TEM micrographs (stained negatively with PTA) of **4b** collected after drop deposition onto carbon-coated copper grids from pH 5.8 (left), pH 7.2 (middle), and pH 8.6 (right) buffer solutions (5 mM with 5 mM of NaCl), respectively.

dx.doi.org/10.1021/ja200182t |*J. Am. Chem. Soc.* 2011, 133, 8534–8543

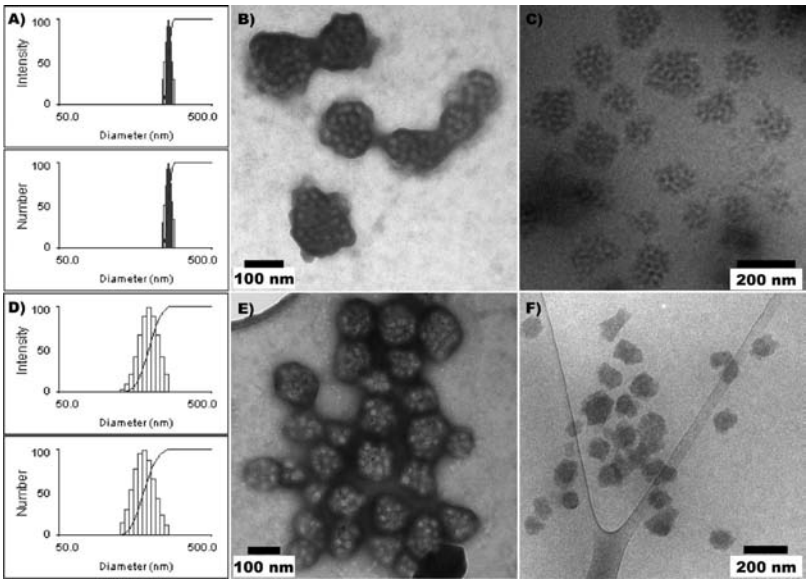

Figure 5. Characterization of MCNs prepared from PEO_{45}-*b*-$PNAS_{105}$-*b*-PS_{45} precursors and cross-linked with **3** in pH 7.2 5 mM PBS buffer (with 5 mM of NaCl, polymer concentrations were 0.2−0.3 mg/mL). (A−C) and (D−F) Hydrodynamic diameter histograms measured by DLS (the scale of *x*-axis was presented by logarithmic), TEM micrograph (stained negatively with PTA), and cryo-TEM micrograph of **5a** and **5b**, respectively.

RESULTS AND DISCUSSION

ABC linear triblock terpolymers have been shown to undergo greater variability in their assembly behaviors, in comparison to diblock copolymers.[36−38,41,50,52,53,59,61,67−70] Furthermore, orthogonal cross-linking of the reactive groups preinstalled across either the hydrophilic[71,72] or the hydrophobic[73] block segment have been demonstrated. The particular triblock terpolymer composition and sequence, PEO_{45}-*b*-$PNAS_{105}$-*b*-PS_{45}, were selected to provide a hydrophilic PEO end segment for water dispersibility, a central PNAS segment for reactivity, and a terminal hydrophobic PS segment to provide for nucleation of micellar assemblies in water and provide the ability to trap initial MCM morphologies kinetically. The activated ester functionalities enable chemical modifications to improve the structural stability by incorporating cross-linkers.

MCMs were assembled from **1** in aqueous solution when the polymers were freshly prepared, by introducing water (a selective solvent for PEO) to solutions of the triblock terpolymer in *N*,*N*-dimethylformamide, DMF (a good solvent for all three blocks). The nanoscale MCM assemblies in H_2O/DMF (v/v = 1:1) were characterized immediately by dynamic light scattering (DLS) and transmission electron microscopy (TEM). The DLS results confirmed that uniform nanostructures were obtained (PDI < 0.1, cumulant analysis) with a hydrodynamic diameter (D_h) of 300 ± 20 nm (Figure 1A). The internal compartmentalized structure of these assemblies was supported by the TEM image (Figure 1B). Distinct from the previous PEO_{45}-*b*-$PNAS_{95}$-*b*-PS_{60} triblock terpolymer, which provided discrete spherical micelles after assembly, the relatively longer PNAS and shorter PS block segments in the current terpolymers caused dramatically different assembly behavior. Individual nanodroplets containing internal phase-segregated domains acquired increasing definition until ultimately dissociating into discrete micelles. We attribute the occurrence of compartmentalization to the difference of interfacial tension of hydrophobic PNAS and PS blocks against water, as the immiscibility of the PNAS and PS segments is not as apparent as prior studies involving other block segment pairs, including fluorophilic blocks.[40,41] Upon inducing the aqueous assembly process, the relatively stronger interfacial tension of PS against water, together with the $\pi-\pi$ stacking interactions between aromatic ring moieties, accelerated the formation of dispersed smaller spherical domains in a larger PNAS domain. The overall progress of internal phase segregation was determined by the intrinsic block length ratio between PNAS and PS blocks. A relatively shorter PS block, which can offer a stronger tendency to spherical morphology, and a relatively longer PNAS block, which grants sufficient space allowing the reorganization of PS and maintains adequate hydrophobicity during the assembly process (at a rate that is slower than the rate of assembly, the NAS groups undergo hydrolysis to generate hydrophilic acrylic acids, AAs (half-life on the order of a few hours)), facilitate the formation of MCMs.

It was noticed that the integrity of the MCM structures was related to the extent of NAS hydrolysis. With increased amounts of AA residues within MCM shells (after 3 months of storage, >95% of the NAS were hydrolyzed, as confirmed by NMR), enhancement of core domain compartmentalization was observed (Figure 1C). Meanwhile, partial dissociation of components within the established MCMs was evidenced by the appearance of smaller aggregates (Figure 1C). These phenomena can be attributed to the increased electrostatic repulsions between negatively charged acrylates. The disassembly of MCMs (without any covalent stabilization) into discrete micellar forms ultimately occurred over long storage times (9 months, Figure 1D). The evolution of the entire process of internal compartmentalization and transformation of MCMs to discrete, amphiphilic core−shell micelles is under further investigation.

The extent of NAS hydrolysis also affected the self-assembly behavior of the triblock terpolymer precursors. Uniform MCMs with a smaller size (D_h = 160 ± 15 nm, Figure 2A) and lower numbers of compartments (Figure 2B) were produced through the assembly of PEO_{45}-*b*-P(NAS_{95}-*co*-AA_{10})-*b*-PS_{45} precursors, having *ca.* 10% NAS hydrolysis. These results sustained our

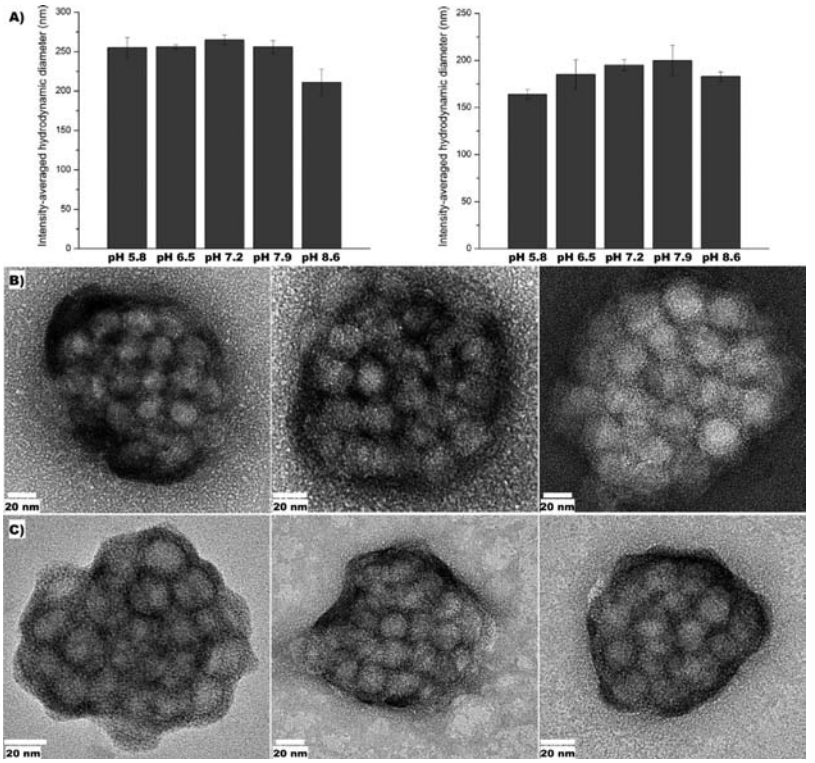

Figure 6. Characterization of MCNs (**5a** and **5b**, polymer concentrations were 0.2−0.3 mg/mL) cross-linked/functionalized by **3**. (A) DLS histograms of intensity-averaged hydrodynamic diameters for **5a** (left) and **5b** (right) in buffer solutions (5 mM with 5 mM of NaCl) at different pH values. (B) High-resolution TEM micrographs (stained negatively with PTA) of **5a** collected after drop deposition onto carbon-coated copper grids from pH 5.8 (left), pH 7.2 (middle), and pH 8.6 (right) buffer solutions (5 mM with 5 mM of NaCl), respectively. (C) High-resolution TEM micrographs (stained negatively with PTA) of **5b** collected after drop deposition onto carbon-coated copper grids from pH 5.8 (left), pH 7.2 (middle), and pH 8.6 (right) buffer solutions (5 mM with 5 mM of NaCl), respectively.

hypothesis (*vide supra*) that the subsistence of charges within MCM shell domains influenced the fate of these supramolecular assemblies and also provided additional tunability for the construction of diverse MCMs. As a note, the triblock terpolymer precursors became only partially soluble in DMF when greater than 30% of NAS hydrolysis had occurred. Therefore, the self-assembly studies of these polymers were not conducted.

Covalent cross-linking and functionalization of the MCMs were accomplished by a one-step approach, utilizing cross-linkers **2** or **3**, designed to also determine the incorporation/cross-linking efficiency[74] and to enable unique pH-driven photophysical property responses.[75] Compared with the MCM precursors, the hydrodynamic diameters of MCNs with cross-linker **2** decreased, as confirmed by DLS (Figure 3A and 3D; also see Figure 4A). The observed shrinkage effect correlated with the cross-linking extents; i.e., as the extents of pyrazine incorporation increased from 0% to 9% to 17%, the corresponding D_h decreased from 300 ± 20 nm to 225 ± 25 nm to 165 ± 30 nm. It also was found that the workup procedure affected the final size for the MCNs with 9% of cross-linking (Figure 4A, left). Although the MCNs retained a similar size of ∼220 nm over a pH range of 5.8 to 7.9, with a further increase of the pH value to 8.6, the hydrodynamic diameter decreased to ∼160 nm. The cause for this reduction in dimension with the increase of pH is unknown. The DLS observations were further supported by high-resolution TEM images of the corresponding MCNs, in which the internal PS compartments in MCNs at pH 8.6 showed a relatively compacted packing mode (Figure 4B). This reduction was tightly associated with the cross-linking extents; at higher degrees of cross-linking, the pH-responsive shrinkage was diminished (Figure 4A, left vs right and Figure 4B vs Figure 4C). However, we are unable to determine whether the apparent reduction in size is due to a contraction within established MCNs or due to some degree of dissociation of loosely cross-linked components within MCNs. These trends were also observed for cross-linker **3** (Figure 5A and 5D, Figure 6A−C). Interestingly, the incorporation efficiency of **3** (∼60%) was higher than that of **2** (∼40%) at both examined cross-linking extents, in contrast to constant relative incorporation of each cross-linker within core−shell micelle systems studied previously.[74]

TEM and cryogenic-TEM (cryo-TEM) imaging (middle and right column in Figures 3 and 5, respectively) of MCNs gave diameters that were in agreement with the DLS results and provided more structural information (also see Figures 4 and 6, Supporting Information, SI, Figures S1 and S2 for TEM images at additional pH values). Comparison of MCM and MCN images (Figure 1 vs 3−6) demonstrated maintenance of the internal segregated domains and enhanced compartmentalization after cross-linking. However, different packing patterns of the compartments occurred with different cross-linking extents. Noticeably different intercompartment spacings were detected by cryo-TEM (Figures 3C, F and 5C, F).

We further characterized the MCNs by atomic force microscopy (AFM). As shown in Figure 7, MCNs with the highest degree of cross-linking (MCN **5b**, maximum ∼30% of cross-linking) displayed the smallest variations between the diameter

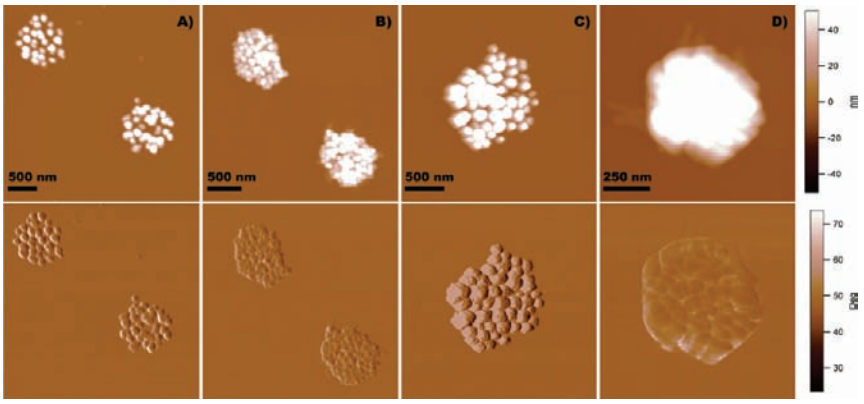

Figure 7. Tapping mode AFM images of MCNs in water (polymer concentrations were 0.2−0.3 mg/mL). (A) Height (top) and phase (bottom) images of **4a** on mica. (B) Height (top) and phase (bottom) images of **4b** on mica. (C) Height (top) and phase (bottom) images of **5a** on mica. (D) Height (top) and phase (bottom) images of **5b** on mica. The AFM samples were prepared by spin-casting the corresponding MCN solution in water on freshly cleaved mica.

and height ($D/H \approx 3$) after casting onto mica, indicating that **5b** had the most discrete and robust structural characteristics. In comparison, the least cross-linked MCN **4a** (maximum ~9% of cross-linking) exhibited a D/H ratio of >8. The AFM images of **4a** vs **4b** and **5a** vs **5b** (Figure 7A vs 7B and 7C vs 7D, respectively) also supplied additional verifications for the general trend of MCN internal structures, i.e., the decrease of inter-compartment spacings with the increase of cross-linking extents.

Small-angle X-ray scattering (SAXS) was then used to probe the internal packing orders of these MCNs (Figure 8). For both cross-linkers, MCNs **4b** and **5b** with higher cross-linking extents showed more ordered internal structures than did **4a** and **5a**, as evidenced by the sharp Bragg peaks (marked with black arrows). The relative positions of the principal Bragg peak (0.024 and 0.022 $Å^{-1}$ for **4b** and **5b**, respectively) to its higher order reflection indicated hexagonal internal packings.[76] The calculated center-to-center spacing was 30.7 nm for **4b** and 33.0 nm for **5b**, respectively. The calculation showed that MCNs prepared using **2** had a smaller spacing than those prepared using **3**, in support of the ability to tune the internal spacing of MCNs by choosing cross-linkers with different chemical structures. For the 20% cross-linked samples (**4a** and **5a**), their SAXS profiles showed broad Bragg peaks, suggesting that these MCNs were less internally ordered, consistent with TEM, cryo-TEM, and AFM images.

The significant increase of MCN structural stability after cross-linking was verified by comparing morphologies of the pre-established MCMs and **2**-cross-linked MCNs (**4a** and **4b**) in mixed organic/aqueous media (DMF/H_2O) over storage times (9 months) at room temperature. While the disassembly of MCMs occurred (*vide supra*), the MCNs (**4a** and **4b**) did not show appreciable morphology variations (Figure S3A and S3B, respectively), even at lower degrees of cross-linking (**4a**, maximum cross-linking extent less than 10%). The long-term dissociation of MCMs into discrete micelles supports our hypothesis that the overall process involves an evolution from multicompartment nanostructures, rather than an opposite process of micellar aggregation.

One motivation for this study arose from our recently reported fluorophore-shell-cross-linked nanoparticles (SCKs), a pH-driven nanoplatform that demonstrated notable enhancement of fluorescent properties within the physiological pH region.[75]

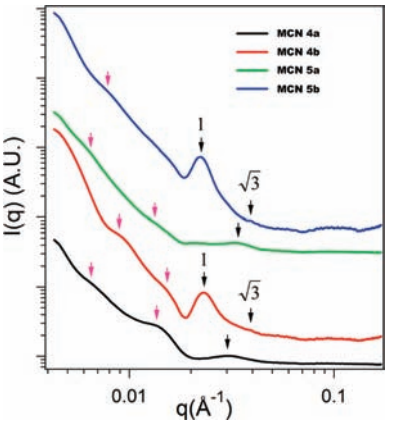

Figure 8. SAXS profiles of MCNs in pH 7.2 PBS buffer solutions (5 mM with 5 mM of NaCl). Black arrows point to the positions of Bragg peaks corresponding to the internal order within the MCNs, while pink arrows mark the positions of possible form factor peaks associated with the overall size of the MCNs.

Because the MCNs represent sophisticated supramolecular assemblies, it was reasonable to anticipate more complex photophysical properties of fluorogenic MCNs after covalent installation of the pyrazine chromophores. For **2** and **3** small molecules at the surveyed pH values, no apparent UV−vis absorbance and fluorescence emission spectra variation was detected (Figure S4), which indicated their intrinsic non-pH-responsive properties. As **2** and **3** were incorporated into MCNs through covalent functionalization, the UV−vis maximum absorbance peaks were blue-shifted from 433 nm to *ca.* 390 and 380 nm (**4a**−**b** and **5a**−**b**, respectively) at pH 5.8. With an increase of the external pH values, the 433 nm peak began to appear along the UV−vis profile and, eventually, became the equivalent or even dominant absorbance peak, depending upon the incorporation extents (Figure 9A−D, left column). More interestingly, the fluorescence emission (excitation at maximum absorbance wavelength, $\lambda_{abs,max}$) at corresponding pH values also experienced such a tendency (Figure 9A−D, middle column). Upon excitation of **4a** in acidic media (pH 5.8 and 6.5, respectively) with $\lambda_{abs,max}$, the fluorescence emission peaks were blue-shifted to 495 nm as the dominant (pH 5.8) or major (pH 6.5) peak. As the environmental

dx.doi.org/10.1021/ja200182t |*J. Am. Chem. Soc.* 2011, 133, 8534–8543

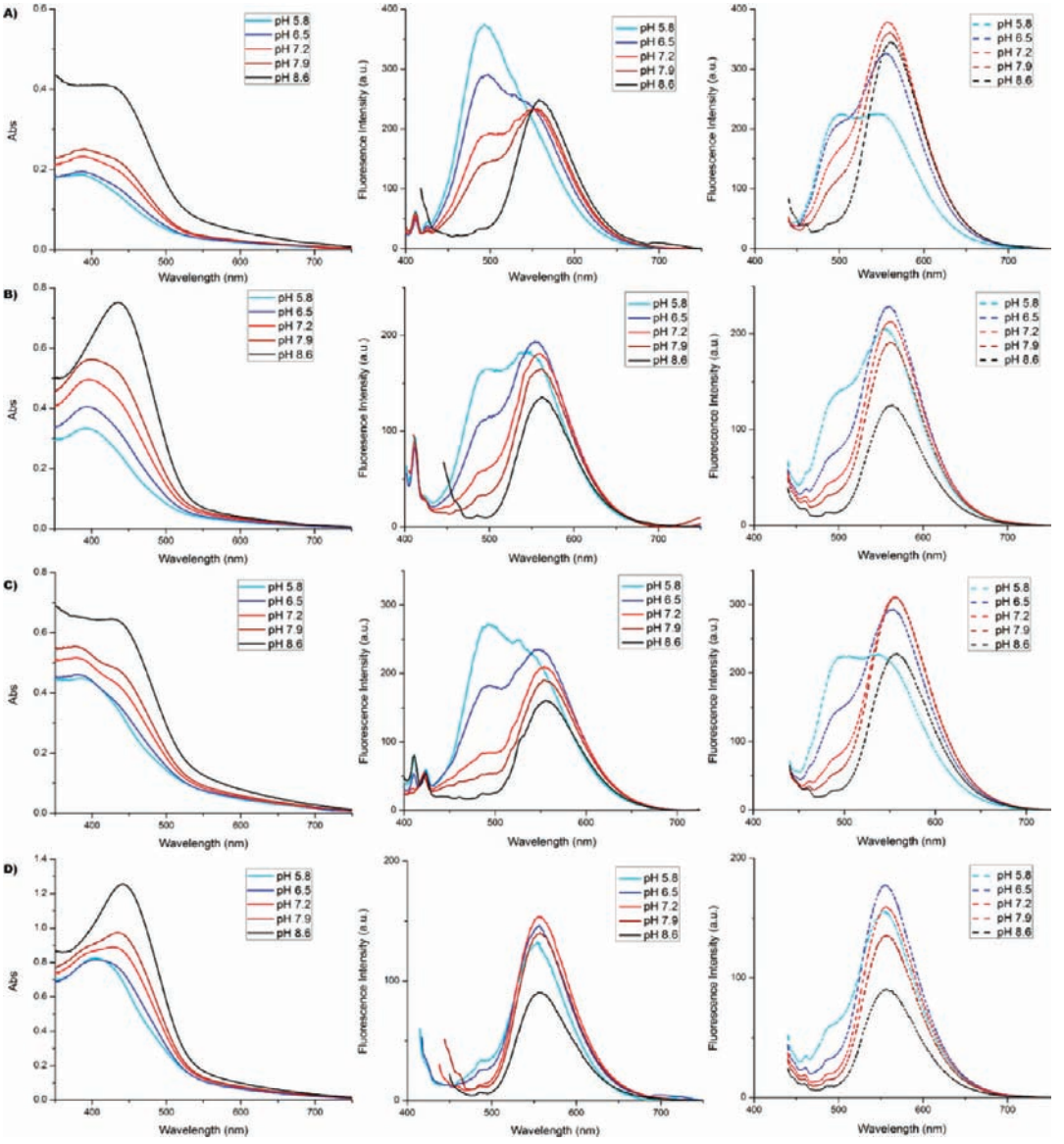

Figure 9. pH-Responsive photophysical properties of cross-linked MCNs. (A−B) UV−vis (left) and fluorescence emission spectra (middle, excitation at $\lambda_{abs,max}$ of MCNs, solid line; right, excitation at 433 nm, dashed line) of MCNs prepared from cross-linking with **2** at nominal 20% and 50% cross-linking extents, respectively. (C−D) UV−vis (left) and fluorescence emission spectra (middle, excitation at $\lambda_{abs,max}$ of MCNs, solid line; right, excitation at 433 nm, dashed line) of MCNs prepared from cross-linking with **3** at nominal 20% and 50% cross-linking extents, respectively.

pH values increased to neutral (pH 7.2) and weakly basic (pH 7.9), **4a** showed dual emissions at 495 and 555 nm, and the 555 nm emissions became of greater intensity at both pH values. At the highest pH value (pH 8.6) surveyed, **4a** only displayed the 555 nm emission. For **5a**, a similar evolution of photophysical properties was verified, except that the threshold of fluorescence emission variation began at pH 6.5 and self-quenching of fluorescence emission was boosted. In the case of **4b**, apparent fluorescence self-quenching appeared and the 495 nm emission quickly vanished as the external pH values were above neutral conditions, in contrast to **4a**. For **5b** with the highest incorporation extent of pyrazines, the 555 nm emission always acted as the dominant character across the surveyed pH range.

We also noticed that, for MCNs **4a**, **4b**, and **5a**, the integrations of the fluorescence emission spectra (excitations at the corresponding $\lambda_{abs,max}$) decreased with the elevation of pH values (Figure 9A−C, middle column), suggesting the existence of two types of fluorogenic species from the covalent installation of pyrazines into the established MCMs. We speculated that these two fluorophores exhibited different photophysical properties as a function of pH; i.e., one had a higher degree of pH-sensitive fluorescence character, which was responsible for the 495 nm emission, while the other one that gave the 555 nm emission had less sensitivity upon pH variations or even was non-pH-sensitive. This hypothesis was supported by the results from studies in which the 433 nm excitations (the original $\lambda_{abs,max}$ for both **2** and **3**) were applied to these fluorogenic MCNs. The reduction of fluorescence emission intensity at 495 nm followed the trend as described above (Figure 9A−D, right column), while significant enhancements of the 555 nm emissions (the $\lambda_{em,max}$ for both **2** and **3**) were observed, for **4a** and **5a**.

dx.doi.org/10.1021/ja200182t |*J. Am. Chem. Soc.* 2011, 133, 8534–8543

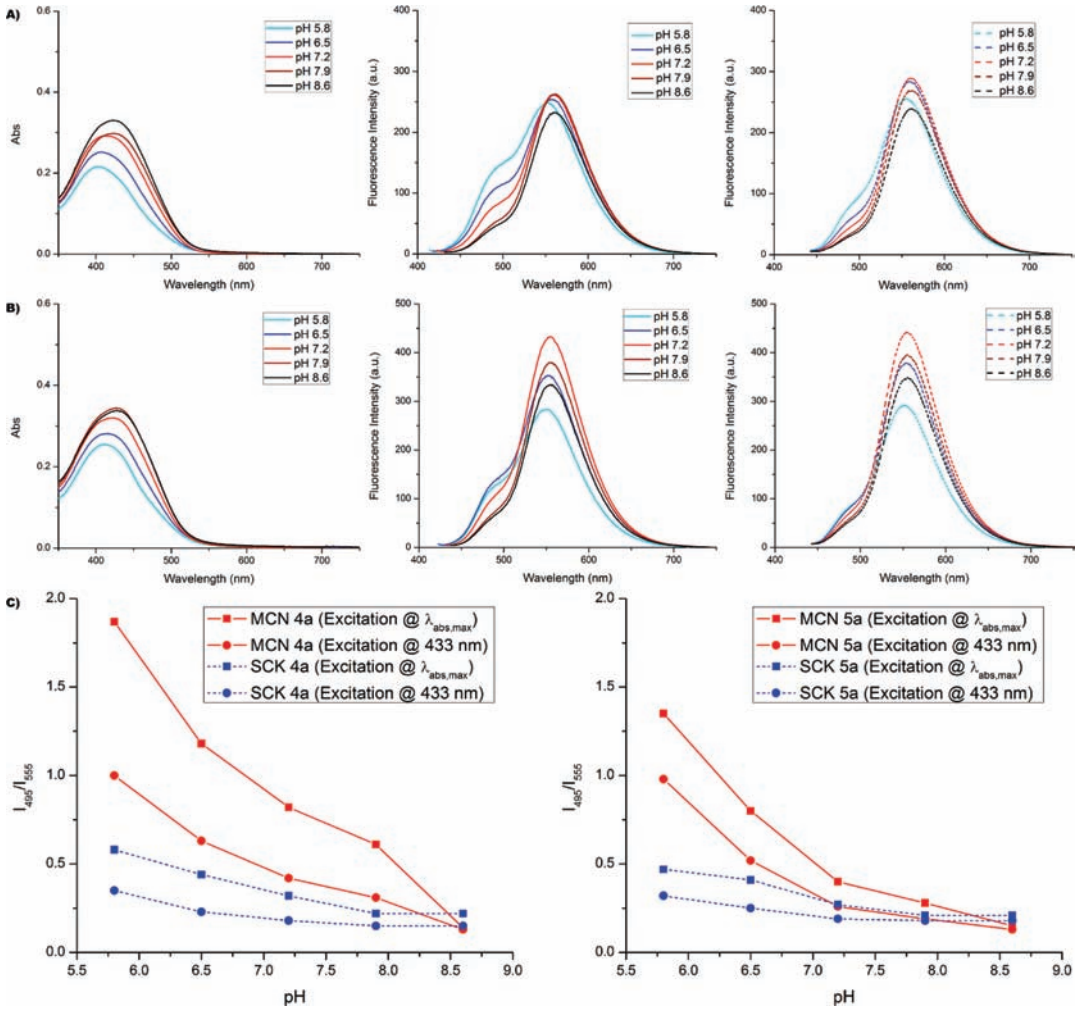

Figure 10. Photophysical properties of photonic SCK nanoparticles. (A–B) UV–vis (left) and fluorescence emission spectra (middle, excitation at $\lambda_{abs,max}$ of SCKs, solid line; right, excitation at 433 nm, dashed line) of SCK **4a** and SCK **5a**, prepared from cross-linking with **2** and **3** at nominal 20% cross-linking extents, respectively. (C) Fluorescence emissions of MCNs and SCKs as a function of environmental pH values (the *y*-axis was presented by the ratio between 495 nm emission intensity and 555 nm emission intensity).

From the chemistry viewpoint, monoacylation of the pyrazine aromatic amines can introduce asymmetries, which might affect its photophysical properties. Therefore, we synthesized the triacylated derivative of **3** (Figure S5) and studied its photophysical properties within the corresponding pH value range. The blue shifts of both the UV–vis maximum absorbance peak (from 433 to 400 nm, Figure S5C) and fluorescence emission peak (from 560 to 495 nm, Figure S5D) were noticed, which was consistent with an earlier literature report.[77] In addition, pH-responsive fluorescence intensity decreases were observed, in response to the increasing of pH from 5.8 to 8.6. This control experiment demonstrated that the pH-sensitive photophysical response by MCNs originated from the acylation of pyrazine aromatic amines. However, other factors including photon reabsorption and subsequent photon re-emission, twisted intramolecular charge-transfer,[78−80] and the ionic strength of the media could also be factors.

To explore the nanostructure morphological effect on photophysical properties, we prepared photonic core–shell SCKs (SCK **4a** and SCK **5a**, at nominal 20% of cross-linking with **2** and **3**, control samples for MCN **4a** and MCN **5a**, respectively) from PEO_{45}-*b*-$PNAS_{95}$-*b*-PS_{60} triblock terpolymer precursors, by following the established protocol.[74] As shown in Figures S6 and S7, these SCK nanoparticles exhibited discrete spherical morphologies and relatively narrow size distributions. Upon exposing these SCKs to photophysical studies, similar pH-responsive fluorescence emission trends were observed as for the MCNs; i.e., the 495 nm fluorescence emission intensity decreased with the elevated environmental pH values (Figure 10). However, the 495 nm emission intensities of SCK **4a** and SCK **5a** were much less than those of the corresponding MCN **4a** and **5a**, especially at acidic conditions (cyan profiles in Figure 10 vs Figure 9). In fact, the 555 nm emission always acted as the major fluorescence emission for all SCK samples, which was totally different from the phenomena observed from MCNs (Figure 10C).

■ CONCLUSIONS

In summary, multicompartment nanoasssemblies bearing NHS active ester functionalities have been prepared from linear triblock terpolymer PEO_{45}-*b*-$PNAS_{105}$-*b*-PS_{45} in DMF/H_2O

dx.doi.org/10.1021/ja200182t |*J. Am. Chem. Soc.* 2011, 133, 8534–8543

solutions and transformed into robust, pH-responsive, fluorescent nanostructures. The phase segregation process between the two hydrophobic building blocks was enhanced by the introduction of hydrophilic functionalities across the PNAS domain, upon hydrolysis, which further provided manipulation of the size and number of internal compartments of the assembled MCMs. The active ester functionalities were demonstrated to allow for modifications through facile and practical chemistry, including cross-linking and functionalizing with pyrazine-based cross-linkers to achieve enhanced stability and to enable pH-sensitive photophysical responses. It is expected that the above unique properties of these MCNs will make them promising materials for fundamental study in biotechnology and other applications.

■ ASSOCIATED CONTENT

Supporting Information. Detailed experimental descriptions including polymer synthesis and self-assembly, functionalized/cross-linked MCN preparation and characterizations, and photophysical evaluations. This material is available free of charge via Internet at http://pubs.acs.org.

■ AUTHOR INFORMATION

Corresponding Author
wooley@chem.tamu.edu

■ ACKNOWLEDGMENT

This material is partially based upon work supported by the National Heart, Lung and Blood Institute of the National Institutes of Health as a Program of Excellence in Nanotechnology (HL080729 and HHSN268201000046C). Financial support from Covidien is gratefully acknowledged. K.L.W. serves as a consultant to Covidien. N.S.L. thanks GlaxoSmithKline for their financial support through an ACS Division of Organic Chemistry Graduate Fellowship. The authors thank Dr. Hamsoo Kim, at the Microscopy and Imaging Center at Texas A&M University, for assistance with high resolution TEM imaging and helpful discussions. Acknowledgement is also made to Washington University School of Medicine, Department of Otolaryngology, Research Center for Auditory and Visual Studies funded by NIH P30 DC004665, Northwestern University, and Argonne National Laboratories for the access to EM and SAXS facilities.

■ REFERENCES

(1) *Block Copolymers in Nanoscience*; Lazzari, M., Liu, G., Lecommandoux, S., Ed.; Wiley-VCH: Weinheim, 2006.
(2) Mecke, A.; Dittrich, C.; Meier, W. *Soft Matter* **2006**, *2*, 751–759.
(3) Nishiyama, N.; Kataoka, K. *Pharmacol. Ther.* **2006**, *112*, 630–648.
(4) Black, C. T. *ACS Nano* **2007**, *1*, 147–150.
(5) Olson, D. A.; Chen, L.; Hillmyer, M. A. *Chem. Mater.* **2008**, *20*, 869–890.
(6) Bang, J.; Jeong, U.; Ryu, D. Y.; Russell, T. P.; Hawker, C. J. *Adv. Mater.* **2009**, *21*, 4769–4792.
(7) van Dongen, S. F. M.; de Hoog, H.-P. M.; Peters, R. J. R. W.; Nallani, M.; Nolte, R. J. M.; van Hest, J. C. M. *Chem. Rev.* **2009**, *109*, 6212–6274.
(8) Segalman, R. A.; McCulloch, B.; Kirmayer, S.; Urban, J. J. *Macromolecules* **2009**, *42*, 9205–9216.
(9) Mikhail, A. S.; Allen, C. *J. Controlled Release* **2009**, *138*, 214–223.
(10) Kim, H.-C.; Park, S.-M.; Hinsberg, W. D. *Chem. Rev.* **2010**, *110*, 146–177.
(11) Tyrrell, Z. L.; Shen, Y.; Radosz, M. *Prog. Polym. Sci.* **2010**, *35*, 1128–1143.
(12) Euliss, L. E.; DuPont, J. A.; Gratton, S.; DeSimone, J. *Chem. Soc. Rev.* **2006**, *35*, 1095–1104.
(13) Champion, J. A.; Katare, Y. K.; Mitragotri, S. *J. Controlled Release* **2007**, *121*, 3–9.
(14) Blanazs, A.; Armes, S. P.; Ryan, A. J. *Macromol. Rapid Commun.* **2009**, *30*, 267–277.
(15) Yoo, J. W.; Chambers, E.; Mitragotri, S. *Curr. Pharm. Des.* **2010**, *16*, 2298–2307.
(16) Geng, Y.; Dalhaimer, P.; Cai, S.; Tsai, R.; Tewari, M.; Minko, T.; Discher, D. E. *Nat. Nanotechnol.* **2007**, *2*, 249–255.
(17) Zhang, K.; Rossin, R.; Hagooly, A.; Chen, Z. Y.; Welch, M. J.; Wooley, K. L. *J. Polym. Sci., Part A: Polym. Chem.* **2008**, *46*, 7578–7583.
(18) Sharma, G.; Valenta, D. T.; Altman, Y.; Harvey, S.; Xie, H.; Mitragotri, S.; Smith, J. W. *J. Controlled Release* **2010**, *147*, 408–412.
(19) Bielawski, C. W.; Grubbs, R. H. *Prog. Polym. Sci.* **2007**, *32*, 1–29.
(20) Tsarevsky, N. V.; Matyjaszewski, K. *Chem. Rev.* **2007**, *107*, 2270–2299.
(21) Sciannamea, V.; Jerome, R.; Detrembleur, C. *Chem. Rev.* **2008**, *108*, 1104–1126.
(22) York, A. W.; Kirkland, S. E.; McCormick, C. L. *Adv. Drug Delivery Rev.* **2008**, *60*, 1018–1036.
(23) Boyer, C.; Bulmus, V.; Davis, T. P.; Ladmiral, V.; Liu, J.; Perrier, S. *Chem. Rev.* **2009**, *109*, 5402–5436.
(24) Kiesewetter, M. K.; Shin, E. J.; Hedrick, J. L.; Waymouth, R. M. *Macromolecules* **2010**, *43*, 2093–2107.
(25) Lodge, T. P.; Bang, J.; Li, Z.; Hillmyer, M. A.; Talmon, Y. *Faraday Discuss.* **2004**, *128*, 1–12.
(26) Soo, P. L.; Eisenberg, A. *J. Polym. Sci., Part B: Polym. Phys.* **2004**, *42*, 923–938.
(27) Harada, A.; Kataoka, K. *Prog. Polym. Sci.* **2006**, *31*, 949–982.
(28) Darling, S. B. *Prog. Polym. Sci.* **2007**, *32*, 1152–1204.
(29) Ryu, J.-H.; Hong, D.-J.; Lee, M. *Chem. Commun.* **2008**, 1043–1054.
(30) Toomey, R.; Tirrell, M. *Annu. Rev. Phys. Chem.* **2008**, *59*, 493–517.
(31) Wurm, F.; Kilbinger, A. F. M. *Angew. Chem., Int. Ed.* **2009**, *48*, 8412–8421.
(32) Kale, T. S.; Klaikherd, A.; Popere, B.; Thayumanavan, S. *Langmuir* **2009**, *25*, 9660–9670.
(33) Zhou, Y.; Yan, D. *Chem. Commun.* **2009**, 1172–1188.
(34) Hayward, R. C.; Pochan, D. J. *Macromolecules* **2010**, *43*, 3577–3584.
(35) Liu, X.; Kim, J.-S.; Wu, J.; Eisenberg, A. *Macromolecules* **2005**, *38*, 6749–6751.
(36) Cui, H. G.; Chen, Z. Y.; Zhong, S.; Wooley, K. L.; Pochan, D. J. *Science* **2007**, *317*, 647–650.
(37) Dupont, J.; Liu, G. J.; Niihara, K.; Kimoto, R.; Jinnai, H. *Angew. Chem., Int. Ed.* **2009**, *48*, 6144–6147.
(38) Chen, Z.; Cui, H.; Hales, K.; Li, Z.; Qi, K.; Pochan, D. J.; Wooley, K. L. *J. Am. Chem. Soc.* **2005**, *127*, 8592–8593.
(39) Erhardt, R.; Zhang, M.; Böker, A.; Zettl, H.; Abetz, C.; Frederik, P.; Krausch, G.; Abetz, V.; Müller, A. H. E. *J. Am. Chem. Soc.* **2003**, *125*, 3260–3267.
(40) Li, Z.; Kesselman, E.; Talmon, Y.; Hillmyer, M. A.; Lodge, T. P. *Science* **2004**, *306*, 98–101.
(41) Kubowicz, S.; Baussard, J.-F.; Lutz, J.-F.; Thuenemann, A. F.; von Berlepsch, H.; Laschewsky, A. *Angew. Chem., Int. Ed.* **2005**, *44*, 5262–5265.
(42) Talingting, M. R.; Munk, P.; Webber, S. E.; Tuzar, Z. *Macromolecules* **1999**, *32*, 1593–1601.
(43) Shen, H.; Zhang, L.; Eisenberg, A. *J. Am. Chem. Soc.* **1999**, *121*, 2728–2740.
(44) Lutz, J.-F.; Laschewsky, A. *Macromol. Chem. Phys.* **2005**, *206*, 813–817.

(45) Li, Z.; Hillmyer, M. A.; Lodge, T. P. *Macromolecules* **2006**, *39*, 765–771.
(46) Li, Z.; Hillmyer, M. A.; Lodge, T. P. *Langmuir* **2006**, *22*, 9409–9417.
(47) Mao, J.; Ni, P.; Mai, Y.; Yan, D. *Langmuir* **2007**, *23*, 5127–5134.
(48) Stavrouli, N.; Triftaridou, A. I.; Patrickios, C. S.; Tsitsilianis, C. *Macromol. Rapid Commun.* **2007**, *28*, 560–566.
(49) Liu, C.; Hillmyer, M. A.; Lodge, T. P. *Langmuir* **2008**, *24*, 12001–12009.
(50) Fang, B.; Walther, A.; Wolf, A.; Xu, Y.; Yuan, J.; Müller, A. H. E. *Angew. Chem., Int. Ed.* **2009**, *48*, 2877–2880.
(51) Gohy, J.-F.; Ott, C.; Hoeppener, S.; Schubert, U. S. *Chem. Commun.* **2009**, 6038–6040.
(52) Schacher, F.; Walther, A.; Ruppel, M.; Drechsler, M.; Müller, A. H. E. *Macromolecules* **2009**, *42*, 3540–3548.
(53) von Berlepsch, H.; Böttcher, C.; Skrabania, K.; Laschewsky, A. *Chem. Commun.* **2009**, 2290–2292.
(54) Saito, N.; Liu, C.; Lodge, T. P.; Hillmyer, M. A. *Macromolecules* **2008**, *41*, 8815–8822.
(55) Skrabania, K.; Laschewsky, A.; von Berlepsch, H.; Böttcher, C. *Langmuir* **2009**, *25*, 7594–7601.
(56) Walther, A.; Müller, A. H. E. *Chem. Commun.* **2009**, 1127–1129.
(57) Skrabania, K.; von Berlepsch, H.; Böttcher, C.; Laschewsky, A. *Macromolecules* **2010**, *43*, 271–281.
(58) Liu, C.; Hillmyer, M. A.; Lodge, T. P. *Langmuir* **2009**, *25*, 13718–13725.
(59) Schacher, F.; Walther, A.; Müller, A. H. E. *Langmuir* **2009**, *25*, 10962–10969.
(60) Saito, N.; Liu, C.; Lodge, T. P.; Hillmyer, M. A. *ACS Nano* **2010**, *4*, 1907–1912.
(61) Walther, A.; Barner-Kowollik, C.; Müller, A. H. E. *Langmuir* **2010**, *26*, 12237–12246.
(62) Lodge, T. P.; Rasdal, A.; Li, Z.; Hillmyer, M. A. *J. Am. Chem. Soc.* **2005**, *127*, 17608–17609.
(63) Uchman, M.; Stěpánek, M.; Procházka, K.; Mountrichas, G.; Pispas, S.; Voets, I. K.; Walther, A. *Macromolecules* **2009**, *42*, 5605–5613.
(64) Hawker, C. J.; Wooley, K. L. *Science* **2005**, *309*, 1200–1205.
(65) Iha, R. K.; Wooley, K. L.; Nyström, A. M.; Burke, D. J.; Kade, M. J.; Hawker, C. J. *Chem. Rev.* **2009**, *109*, 5620–5686.
(66) Krishnamurthy, V. M.; Estroff, L. A.; Whitesides, G. M. In *Fragment-based Approaches in Drug Discovery*; Jahnke, W. Erlanson, D. A., Ed.; Wiley-VCH: Weinheim, 2006; pp 11−53.
(67) Zheng, R.; Liu, G. *Macromolecules* **2007**, *40*, 5116–5121.
(68) Hales, K.; Chen, Z. Y.; Wooley, K. L.; Pochan, D. J. *Nano Lett.* **2008**, *8*, 2023–2026.
(69) Hu, J.; Liu, G.; Nijkang, G. *J. Am. Chem. Soc.* **2008**, *130*, 3236–3237.
(70) Sundararaman, A.; Stephan, T.; Grubbs, R. B. *J. Am. Chem. Soc.* **2008**, *130*, 12264–12265.
(71) Bütün, V.; Wang, X. S.; de Paz Báñez, M. V.; Robinson, K. L.; Billingham, N. C.; Armes, S. P.; Tuzar, Z. *Macromolecules* **1999**, *33*, 1–3.
(72) Ma, Q.; Remsen, E. E.; Clark, C. G.; Kowalewski, T.; Wooley, K. L. *Proc. Natl. Acad. Sci. U.S.A.* **2002**, *99*, 5058–5063.
(73) Stewart, S.; Liu, G. *Chem. Mater.* **1999**, *11*, 1048–1054.
(74) Sun, G.; Lee, N. S.; Neumann, W. L.; Freskos, J. N.; Shieh, J. J.; Dorshow, R. B.; Wooley, K. L. *Soft Matter* **2009**, *5*, 3422–3429.
(75) Lee, N. S.; Sun, G.; Neumann, W. L.; Freskos, J. N.; Shieh, J. J.; Dorshow, R. B.; Wooley, K. L. *Adv. Mater.* **2009**, *21*, 1344–1348.
(76) Abbas, S.; Lodge, T. P. *Langmuir* **2008**, *24*, 6247–6353.
(77) Shirai, K.; Yanagisawa, A.; Takahashi, H.; Fukunishi, K.; Matsuoka, M. *Dyes Pigm.* **1998**, *39*, 49–68.
(78) LaFemina, J. P.; Schenter, G. K. *J. Chem. Phys.* **1991**, *94*, 7558–7559.
(79) Gómez, I.; Reguero, M.; Boggio-Pasqua, M.; Robb, M. A. *J. Am. Chem. Soc.* **2005**, *127*, 7119–7129.
(80) Cogan, S.; Zilberg, S.; Haas, Y. *J. Am. Chem. Soc.* **2006**, *128*, 3335–3345.